MAY 1982 LRP 205/82

THE LINEAR MAGNETIZED PLASMA DEVICE

(LMP)

M.Q. Tran, P. Kohler, P.J. Paris and

M.L. Sawley

THE LINEAR MAGNETIZED PLASMA DEVICE (LMP)

M.Q. Tran, P. Kohler, P.J. Paris, and M.L. Sawley

Centre de Recherches en Physique des Plasmas
Association Euratom - Confédération Suisse
Ecole Polytechnique Fédérale de Lausanne
21, Av. des Bains, CH-1007 Lausanne/Switzerland

Abstract

This report is to serve as an introduction to the LMP device, giving details of its design, construction and plasma parameter values as well as the experiment for which it is planned to be initially used.

The report is subdivided into three main sections. In the first section, the constituent elements (magnetic field coils, vacuum vessel and plasma source) of the LMP device are described. The remaining two sections are devoted to a description of the proposed initial experiment to be conducted on the device; an investigation of the ponderomotive force exerted by an ion cyclotron wave on a two-ion species plasma. Section two outlines the general physics considerations that were taken into account in designing this experiment, while section three describes the Doppler-free laser spectroscopy diagnostic technique that is to be used to measure modifications of the spatial distribution of ions resulting from the ponderomotive force.

1. MACHINE DESIGN AND PARAMETERS

1.1 Introduction

In view of the need of a device in which the physics of a magnetized plasma could be studied, the design and construction of the Linear Magnetized Plasma Device (LMP) have been undertaken. The general philosophy that was used as a guideline during the design phase was the flexibility of the machine. In practice, this entails the following considerations:

- the magnetic field should be as high as is possible using the available power supply;
- the volume for which magnetic field homogeneity is reasonably good should be as large as possible, enabling a plasma of sufficiently large diameter;
- the diagnostic access to the device must be good.

The first condition (the highest magnetic field compatible with the existing power supply) is necessary if one wishes to study waves of frequency in the vicinity of the ion cyclotron frequency. The requirement that the ion Larmor radius must be much smaller than the plasma diameter yields the second condition. A large plasma diameter would be necessary if waves propagating perpendicular to the magnetic field were to be studied (e.g. electrostatic ion cyclotron waves). The condition of good diagnostic access involves some compromise with that of magnetic field homogeneity.

Another consideration was taken into account in selecting the length of the machine. The proposed first experiment (the effect of the ponderomotive force due to an ion cyclotron wave) required that the machine be long enough to accommodate more than one wavelength.

The design parameters of the machine are presented in table I. A general view of the machine is presented in Fig. 1. Detailed discussion of the main machine components will be given in the following sub-sections.

1.2 Magnetic field

A linear homogeneous magnetic field (design field homogeneity ≃ 0.3% over a length of 4.75 m and a diameter of 0.2m) is created by 44 identical coils. The coil characteristics are given in Table II. With the selected copper bar, a field of 0.3 T can be obtained with a current of 850 A. At an operating temperature of 60 °C, the voltage drop across the whole solenoid is 220 V.

Each coil is formed from two independent two turn, nine layer pancakes which are sandwiched together (Fig. 2). The two separate pancakes are wound in such a way that the axial current component due to the two turn-to-turn transitions cancel.

Each of the pancakes is individually water-cooled. To dissipate the heat generated in one pancake (P = 1.65 kW) a flow rate of 2.6 l/min is required for each pancake. The total pressure drop is approximately 1 bar. The cooling system for the whole solenoid consists of a water pump (flow rate: 120 l/min at 8.6 bars) and a forced air cooled heat exchanger which can dissipate 200 kW.

The current in the solenoid is regulated to compensate for long-term drift. This is achieved through a second 40V - 1000A power supply in series with the main one. It is not necessary to regulate the 300 Hz ripple since the solenoid inductance ($L \simeq 5 \times 10^{-2}$ H) is large enough so that the current fluctuation at 300 Hz is only about 0.01 percent. Fast switching diodes are inserted across the coil terminals to prevent any high voltage development if the circuit is opened accidentally. Thermal switches are also placed at the cooling water inlet and outlet of each pancake and will automatically switch off the power if the temperature exceeds a threshold value (T = 75 °C at the water outlet). The coil power supplies and safety interlocks will be controlled by a micro-processor system.

TABLE II : Coil characteristics

Coil inner diameter	.522 m
Coil outer diameter	.830 m
Number of turns	4
Number of layers	9
Conductor type	Copper OF
Conductor size	20.83 x 15.75 mm^2
Cooling	water flow through a circular hole of diameter 6.35 mm
Typical coil electrical resistance at 20 ° C	4.58 m Ω

1.3 Vacuum system

A) Material

The usual stainless steel AISI 304 was not selected because of its magnetic properties. Although AISI 304 stainless steel is an austenite steel with low ferrite concentration (< 1%), machining and welding causes an increase in the ferrite concentration (up to 10%). This induces local magnetic fields and a variation of the permeability. A sample of 5 mm thickness containing about 5% ferrite along the weld, kindly furnished by the Institut des métaux et machines, has been tested. A maximum magnetic field of 10 gauss was measured on the weld. However, at 10 cm above the weld, the field was not detectable. Variation of the permeability of the order of a percent was measured using a field perpendicular to the weld.

The use of a Schaeffer diagram allows the selection of an acceptable stainless steel. The commercially available AISI 316 L (or 4435 BN2) was chosen. With this steel, a concentration of ferrite less than 1% after welding and machining can be guaranteed by the manufacturer. The wall thickness is 3mm.

B) Vacuum vessel

The philosophy of the design of the vessel was flexibility and modularity. The availability of diagnostic access has been maximized. The 9.2m long, 0.40m diameter vacuum vessel is comprised of nine sections. The two end sections are connected to the pumping systems. Since the pumping system contains components which are ferrite, the length of the end sections is such that these components are in a region where the field created by the solenoid is less than 1% of its central value. The seven other sections have a total of 62 openings. The five central sections, which are within the region of homogeneous magnetic field, offer the possibility of diagnostic access at 88 different axial and azimuthal positions. All of the sections, except the two end connecting sections, are water-cooled, with special emphasis placed on the sections that will house the plasma sources. All the vacuum seals are Viton O-rings. The large flanges which connect the sections together are water-cooled.

If needed, new sections with openings adapted to a specific problem can be ordered at a reasonable price since all the toolings are already available.

C) Pumping system

Two pumping units are installed at the ends of the device. Each consists of a 2600 l/s diffusion pump backed by a 1000 l/min roughing pump. A freon baffle is used to prevent oil back-diffusion. A base pressure of 10^{-7} torr is anticipated.

Ionization gauges will be used to monitor the pressure at the centre and both ends of the vacuum vessel. To avoid perturbation of the central measurement caused by the magnetic field, an extension tube will be used to displace the gauge from the region of high magnetic field: appropriate calibration of the central gauge will be undertaken.

1.4 Plasma sources

A) Review of various plasma sources

Let us first review the various steady-state plasma sources suitable for a laboratory magnetized plasma. One of the best-known is the alkali plasma source used in a Q-device[1]. Neutral alkali vapour is ionized by surface ionization on a hot electron-emitting tungsten plate. The plasma produced is very quiescent. Its density can be as high as $10^{12} cm^{-3}$, the electron and ion temperature are of the order of 0.1 eV. The use of an alkali plasma makes the operation of electrical probes somewhat delicate. The tungsten plate must be at high temperature (around 2000 ° C) with a high degree of uniformity in its temperature. Sophisticated plate-heating designs have been elaborated in the past.

A plasma could also be produced by RF, either resonantly or non-resonantly. Resonant sources use either slow wave structures (Lisitano coils)[2,3] or open waveguides[4] excited at the electron cyclotron frequency f_{ce} (for B = 0.3 T, $f_{ce} \simeq 8.4$ GHz). Non-resonant structures[5] are usually excited at a frequency around a few MHz. Although at low power, quiet plasma production is possible, RF-produced plasmas are notoriously noisy at high RF level (P > 100 W).

Discharge-produced plasmas are widely used. Electron-emitting cathodes are commonly used for plasma diameters up to 1m. The cathode can be a nickel plate coated with either barium oxide or a more exotic material, such as the lanthanum hexaboride (LaB_6). Dispenser cathodes, which consist of a formula of barium oxide dispensed throughout a porous matrix of tungsten, may also be used. An alternative approach[6,7] uses hot tungsten filaments placed in the region where the fringing magnetic field is low enough so that the Larmor radius of the energetic ionizing electrons is smaller than the spacing of the filaments. From simple flux conservation, it is obvious that such a source is only suitable for a plasma having a small diameter or a modest magnetic field.

For the LMP machine, we have decided to use a cathode as a plasma source. Considerably more development would be required if alkali or RF sources with suitable characteristics were to be considered.

B) Source description

A plasma diameter of 5 cm has been chosen. This initial choice has been made to utilize previous experience and expertise with cathodes of this type, as well as being governed by physics considerations of the proposed initial experiment (see section 2). At a later date, the plasma diameter could be increased to 10 cm or more. Densities greater than 10^{10} cm^{-3} are desirable. Neutral gas pressure will be in the range of 10^{-4} Torr. The cathode will have an emission current of up to 15 A continuous or 100 A pulsed.

Our experience with cathodes of nickel plate coated with barium oxide reveals that at emission currents of the order of a few amperes, ion bombardment severely limits their lifetime (of the order of day(s)). In addition, these cathodes deteriorate rapidly in the presence of oxygen. After conditioning, they will not survive frequent openings of the device to normal atmospheric conditions. Dispenser cathodes have proved to be more robust, and are therefore a desirable alternative. However, we also envisage the use of a LaB_6 cathode. The emitting temperature of LaB_6 is 1600 °C. The LaB_6 is held by a graphite support with all insulating pieces constructed from boron nitride. The heat reflector is made of tantalum. The total heat input for a cathode of 5 cm diameter is 2.8 kW. The cathode is biased at a negative potential with the grid fixed at ground potential. The use of a grid of fine tungsten wire mesh is foreseen. If, however, this should yield a plasma column having an unacceptably high level of filamentation (due to the small Larmor radius of the emitted electrons in a 0.3 T magnetic field), the use of a ring anode will be investigated. The cathode design is shown in Fig. 3.

mirror devices[17,18] and the electrostatic flute mode in a bumpy torus[19]. Extensive studies have also been conducted on the use of the ponderomotive force in the radio-frequency plugging of open-ended confinement devices[20-24]. These have investigated the reduction of plasma loss from magnetic cusps due to the non-linear force exerted by an electrostatic RF field in a non-uniform magnetic field. This technique has also been studied as a means of impurity control by preferential plugging of a plasma containing more than one ion species[25,26].

The ponderomotive effect of an electromagnetic wave in a uniformly magnetized plasma containing two ion species has also been examined theoretically[27-29]. It has been shown that a left-circularly polarized wave tends to spatially separate ions of different charge-to-mass ratio if the frequency of the wave lies between their cyclotron frequencies. This result arises due to the form of the ponderomotive potential which, from the single particle analysis of Motz and Watson[16], is given by

$$\phi_p = \frac{q^2}{4m\omega}\left(\frac{E_L^2}{\omega-\omega_c} + \frac{E_R^2}{\omega+\omega_c} + \frac{E_{\parallel}^2}{\omega}\right), \qquad (1)$$

where $E_{\parallel}$, E_L and E_R are, respectively, the amplitudes of the longitudinal, and transverse left and right circularly polarized components of the applied electric field. From this expression it can be seen that the sign of the ponderomotive potential, and hence the direction of the resulting force experienced by an ion (electron) due to a left (right) circularly polarized wave, changes sign as the wave frequency passes through the cyclotron frequency. For a sufficiently large amplitude wave, substantial modification of the ion densities have been calculated both for an unbounded[27,28] and a bounded[29] plasma.

2.2 The LMP experiment

An experimental investigation of the ponderomotive force in a plasma containing two ion species will be the initial objective of the LMP device. To date, there has been no experimental study of the ponderomotive force due to an electromagnetic wave in a uniformly magnetized plasma.

A) Choice of plasma

Estimates of the density modification produced by the ponderomotive force may be obtained using the calculations of Reference 28. For a plasma containing one or more singly-ionized ion species, the modified electron and ion densities due to the ponderomotive force of a plane, left-circularly polarized electromagnetic wave may be written as

$$n_e = n_{eo} \exp\left(\frac{-\phi_e}{T_e+T_i}\right)\left[\sum_\sigma \frac{n_{\sigma o}}{n_{eo}} \exp\left(-\frac{\phi_\sigma}{T_i}\right)\right]^{\frac{T_i}{T_e+T_i}} \qquad (2a)$$

and

$$n_\sigma = n_{\sigma o}\, n_e \exp\left(\frac{-\phi_\sigma}{T_i}\right)\left[\sum_\sigma n_{\sigma o} \exp\left(-\frac{\phi_\sigma}{T_i}\right)\right]^{-1}, \qquad (2b)$$

where

$$\phi_j = \frac{e^2 |E_L|^2}{2 m_j \omega (\omega - \omega_{cj})} . \qquad (2c)$$

Here, each of the ion species σ is assumed to have the same temperature T_i, and the subscript o denotes the density without the wave.

For an ion cyclotron wave, $\omega \simeq \omega_{c\sigma}$, and hence, from eq. (2c), $\phi_e \ll \phi_i$. For the LMP device we also have $T_e \gg T_i$. Equation (2) therefore yields:

- for a plasma containing one ion species:

$$n_i = n_e \simeq n_{eo} \exp\left(-\frac{\phi_i}{T_e}\right), \tag{3}$$

- for a plasma containing two ion species:

$$n_e \simeq \sum_\sigma n_{\sigma o} \exp\left(-\frac{\phi_\sigma}{T_e}\right), \tag{4a}$$

$$n_\sigma \simeq n_{\sigma o} n_{eo} \exp\left(-\frac{\phi_\sigma}{T_i}\right)\left[\sum_\sigma n_{\sigma o} \exp\left(-\frac{\phi_\sigma}{T_i}\right)\right]^{-1}. \tag{4b}$$

If we consider the special case with $n_{10} \gg n_{20}$, $\omega_{c1} > \omega_{c2}$ (appropriate to a neon plasma with Ne^{20} and Ne^{22} in their naturally occurring concentrations) and $\phi_2 \simeq -\phi_1$ (i.e., $\omega \simeq (\omega_{c1} + \omega_{c2})/2$), we obtain from eq. (4b) for the majority ion species

$$n_1 \simeq n_{1o} - n_{2o} \exp\left(-\frac{2\phi_2}{T_i}\right), \tag{5a}$$

while for the minority ion species

$$n_2 \simeq n_{2o} \exp\left(-\frac{2\phi_2}{T_i}\right). \tag{5b}$$

For values appropriate to the parameters of the LMP device, given in section 1, we have

$$T_e \simeq 5|\phi_i| \simeq 25\, T_i \simeq 100|\phi_e|.$$

Equation (3) thus shows that for a single ion species plasma the density modification is not substantial. However, in a two ion species plasma, even though the electron and majority ion species suffer little change in density, there is a large percentage change in the density of the minority ion species.

With these calculations in mind, it is therefore advantageous to investigate the ponderomotive force in a plasma containing two ion species, choosing the wave frequency midway between the two ion cyclotron frequencies. The choice of neon as the working gas was influenced by several considerations:

i) the presence of essentially two isotopes in naturally occurring neon, Ne^{20} and Ne^{22} (% of $Ne^{21} < 0.3\%$), with $n_{o2}(Ne^{22}) \simeq 0.1\ n_{o1}\ (Ne^{20})$.

ii) isotopic masses with ion cyclotron frequencies using the available magnetic field which are compatible with the existing RF power amplifier
ie., for $B_o = 0.3$ T, $\omega_{c1}(Ne^{20}) = 230.4$ kHz
$\omega_{c2}(Ne^{22}) = 209.4$ kHz

iii) enhancement of the ponderomotive potential due to the proximity of the two ion cyclotron frequencies, which however, are distant enough to allow $\omega_{c2} < \omega < \omega_{c1}$ while avoiding significant cyclotron damping of the wave (see section 2.3).

iv) ready availability of neon and relative ease of producing a neon plasma with suitable parameter values.

v) sodium ions, $(Na^{23})^+$, (produced in the form of a beam by an oven) may be used to closely model the behaviour of the minority Ne^{22} ions (see section 3). In addition, by injecting a small amount of argon gas, there exists the possibility of modelling the behaviour of the Ne^{20} ions using doubly ionized argon ions (since $\omega_{ci}(Ar^{40})^{++} \simeq \omega_{ci}(Ne^{20})^+$). These features enable a simplification of the diagnostic analysis of the plasma.

Equation (2) shows that the spatial variation of the modified densities depends on the electric field of the wave through the ponderomotive potential. In a plasma column, where a bounded mode is excited, the distribution of the (minority ion) species should be strongly dependent on spatial location.

B) Antenna design

Since we wish to observe a non-linear effect ($\phi \alpha |E|^2$), large oscillating field amplitudes inside the plasma column are necessary. An efficient method of achieving this goal is to excite an eigenmode of the plasma cavity (rather than use the fringing fields of an antenna). Although it is desirable to excite a pure left-circularly polarized wave to make efficient use of the resonant denominator in the ponderomotive potential, in a bounded geometry this is not possible. However, in general, the mode excited will have a left-circularly polarized component, as well as right-circularly polarized and longitudinal components.

A linear analysis of free and forced ion cyclotron waves in a cylindrical plasma cavity, pertinent to the present experimental investigation, has been considered by Sawley and Tran[30]. For the density range of interest, the magnetoacoustic (fast) wave has much too long a wavelength to be accommodated by the LMP device (λ_{fast} > 5 x length of machine). However, it is shown that an ion cyclotron mode with a convenient wavelength may be excited. A good choice of eigenmode is the ($n = 4$, $\ell = 1$) mode, that is, one with an axial wavelength of half the machine length and a simple radial field distribution. The axial field structure of this mode is suitable for diagnostic analysis at the nodes and antinodes using the ports available on the LMP device. It also has the advantage that since there are two complete axial wavelengths within the device, observation at both nodes and antinodes which are far from the axial boundaries is possible. This is important if the ends of the cavity do not present well-defined boundaries, and therefore affect the fields in their vicinity. Excitation of this mode by a Stix coil has been considered[30], and the power input and resulting wavefields calculated. It has been shown, using a realistic value of wave damping due to ion-neutral collisions, that this wave may be very selectively excited. The electric field is essentially a combination of the E_r eigenmode field and the E_θ vacuum field components. Assuming an antenna resistance of 0.3 Ω, it has been calculated[30] that most of the power input is dissipated in the antenna (plasma resistance = 0.23 m Ω), and a power input of 1 kW yields a

maximum value for the amplitude of the dominant radial electric field component of $|E_r| \simeq 300\ Vm^{-1}$ near the mid-radius position of the plasma.

As noted by Sawley and Tran, using the wavefield of a bounded mode to study ponderomotive force effects has the disadvantage that, for fixed plasma parameters, the eigenfrequency is not a free parameter, but is fixed by the dispersion relation of the wave. The dependence of the ponderomotive force on the difference between the driving frequency and the cyclotron frequency of a given ion species, $\omega - \omega_{ci}$, is therefore not straightforward to examine. However, as shown in Fig. 8 of Reference 30, the eigenfrequency of a particular mode can be altered by changing the relative concentration of the two isotopes which constitute the plasma.

A schematic diagram of the antenna circuit is shown in Fig. 4a. The Stix coil used to excite the $n = 4$ mode consists of four separate coil modules, alternately dephased by 180 degrees (by reversing the direction of current flow) and placed at regular intervals along the device. Each module is 67.5 cm in length and 12 cm in diameter, while the spacing between the centres of neighbouring modules is 135 cm. A more detailed sketch of a module is shown in Fig. 4b. Each module consists of 24 turns of square section copper tubing separated into six sub-coils and joined by straight sections. This design was chosen to avoid reducing the diagnostic access to the region beneath the wave excitation coils: the wave coils are coaxially alligned beneath the main magnetic field coils of the LMP device. The design includes the possibility of a Faraday shield which may be easily inserted or removed. The shield is constructed from a copper tube of thickness greater than the skin depth (at 250 kHz, $\delta = 0.15$ mm), with eight equally-spaced axial cuts along almost the entire length[31]. Each module of the Stix coil is individually water cooled, allowing for steady state operation. The coil is driven, via a capacitor matching circuit, by a 1 kW solid state amplifier (ENI model 1140 LA, flat gain for $9\ kHz < f < 250\ kHz$). The construction of a 20 kW amplifier, which may be used in either continuous or pulsed mode, is also anticipated.

2.3 Possible deleterious effects

There exists a number of processes that are not accommodated by the fluid models used to describe the linear wave behaviour[30] and also the non-linear pondermotive effect[27-29]. These processes may introduce effects that are deleterious for the observation of the density modification caused by the pondermotive force, such as the transfer of wave energy into randomized particle energy, i.e., plasma heating (an increase in the ion temperature causes a decrease in the ratio ϕ/T_i and hence a decrease in the density modification resulting from the ponderomotive force). We shall consider each of these possible processes in turn.

A) Collisional damping

The theoretical model of Weibel and Festeau-Barrioz[29] assumes the plasma is collisionless, that is

$$\nu_c \ll |\omega - \omega_{ci}| \quad . \tag{6}$$

For the weakly ionized plasma of the LMP device it can be shown[30] that the dominant collisional process is ion-neutral collisions. For the expected plasma parameters given in Table I, the ion-neutral collision frequency is approximately $\nu_c \simeq 5$ kHz. Since we require $\omega_{c2} < \omega < \omega_{c1}$ where $(\omega_{c1} - \omega_{c2}) = 21$ kHz, this value of ν_c appears to be higher than desirable. The ponderomotive effect may therefore be reduced due to the unfavourable result of charge-exchange collisions between ions and neutrals of different species randomizing the position and velocity of ions of each species.

It should be noted that since $\nu_c \propto n_n$, the possibility exists of decreasing ν_c by decreasing the background neutral pressure in the device, for example, by gas puffing.

B) Cyclotron damping

To avoid appreciable ion cyclotron damping of the wave, the wave frequency is required to be sufficiently distant from both of the ion cyclotron frequencies, that is

$$k_{\parallel} v_{th,i} \ll |\omega - \omega_{ci}| \tag{7}$$

and also

$$k_{\perp} \rho_{ci} \ll 1. \tag{8}$$

For the chosen plasma and wave parameters,

$$k_{\parallel} v_{th,i} \sim 400 \text{ Hz}$$

and

$$k_{\perp} \rho_{ci} \sim 8 \times 10^{-2}.$$

For a wave frequency approximately midway between the ion cyclotron frequencies of the two neon species, the above inequalities should be sufficiently well satisfied to avoid appreciable cyclotron damping. For frequencies very close to either ion cyclotron frequency, or if there is a substantial increase in the ion temperature due to the wave (resulting in an increase in $v_{th,i}$ and ρ_{ci}), cyclotron damping may become substantial.

C) Landau damping

Landau damping involves energy transfer from the wavefields to particles moving along the magnetic field with the phase velocity of the wave, that is, particles for which $\omega - k_{\parallel} v_{\parallel} = 0$. This damping mechanism is therefore expected to be significant if

$$k_{\parallel} v_{th} \simeq \omega. \tag{9}$$

For the LMP device,

$$k_{\parallel} v_{th,i} \sim 400 \text{ Hz}$$

and

$$k_{\parallel} v_{th,e} \sim 200 \text{ kHz}.$$

Therefore, while ion Landau damping should be insignificant for the ion cyclotron wave under consideration, electron Landau damping may play a dominant role.

To obtain an estimate of the magnitude of electron Landau damping for the proposed LMP experiment, we may calculate the damping rate γ (where γ is the imaginary part of the complex eigenfrequency) under the assumption that $\gamma \ll \omega_o$ (ω_o being the eigenfrequency obtained from cold plasma theory). Writing the dispersion relation for the ion cyclotron wave as

$$D_o + i\, D_1 = 0$$

where D_o is the cold plasma term and D_1 includes the additional terms due to collisionless damping, we find

$$\gamma \simeq \frac{D_1(\omega_o)}{\left.\frac{\partial D_o}{\partial \omega}\right|_{\omega_o}} \quad . \tag{10}$$

For the parameter regime of interest we obtain, assuming an infinite plasma,

$$D_1(\omega_o) \simeq i\, n_x^2 \left(K_{xx} - n_z^2 \right) \Delta K_{zz}$$

and

$$\left.\frac{\partial D_o}{\partial \omega}\right|_{\omega_o} \simeq - n_x^2 \left(K_{zz} - n_x^2 \right) \Delta D_o \quad ,$$

where

$\underline{\underline{K}}$ is the cold plasma dielectric tensor,

$\Delta\underline{\underline{K}}$ is a tensor containing the additional collisionless damping terms[32]

and

$$\Delta D_o = \frac{c^2}{\omega^2} \sum_s \frac{2\,\omega_{ps}^2\,\omega_{cs}^2}{\omega\,(\omega_{cs}^2 - \omega^2)^2} \quad .$$

Substituting into eq. (10) the appropriate values for the plasma of the LMP device yields $\gamma \simeq \omega_o$, indicating that electron Landau damping may be substantial. (Under these conditions a reliable value of γ cannot be obtained using the present perturbation approach that assumes $\gamma \ll \omega_o$.)

It should be noted that there is a fundamental difference between ion-neutral collisions (discussed in section 2.2 A) and electron Landau damping, in connection with the ponderomotive effect under consideration. Both processes broaden the resonance curve and increase the power input to the plasma required to obtain wavefields of suitable amplitude, however, electron Landau damping does not directly randomize the position and velocity of ions of a particular species as does charge exchange with neutrals of the other species. Since only a small fraction of the power input into the system is dissipated in the plasma by ion-neutral collisions (see section 2.2 B), maintaining a sufficiently large amplitude mode should not be prohibitive even in the presence of additional electron Landau damping.

The additional power input results in heating of the electrons. Since the electron self collision time[33], $\tau_{ee} \simeq 3 \times 10^{-6}$s, is of the same order as the transit time for electrons along the length of the device, an increase in electron temperature due to Landau damping is to be expected. However, since the equipartition time[33] between electrons and ions, $\tau_{eq} \simeq 5 \times 10^{-2}$s, is much more than the ion transit time along the length of the device, no significant increase in the temperature of the ion species should result.

Therefore, although electron Landau damping may cause an increase in the plasma loading and electron temperature, this mechanism should not be deleterious to the observation of the ponderomotive effect since the increase in ion temperature is expected to be minimal.

D) Transit-time effects

The standard expression for the ponderomotive potential given in eq. (1) is valid if the gradient scale length, ℓ, of the electric field is large compared to the ratio $v/(\omega-\omega_c)$, where v is the component of the particle velocity in the direction of the field gradient[16]. If the wave frequency is sufficiently close to the cyclotron frequency, a particle will not respond adiabatically to the electric field.

Such non-adiabatic, transit-time effects have been studied theoretically and experimentally by Dimonte et al.[34,35]. By considering the single particle motion of ions in the electrostatic field of a pair of parallel plates, it has been shown that at $\omega = \omega_{ci}$ the ponderomotive potential is small, rather than singular as given by eq. (1). The maximum in the potential occurs at the transition from the non-adiabatic to the adiabatic regime. For an admixture of two ion species, a relationship has been derived[35] which must be satisfied for the ions to respond adiabatically to an electric field of frequency midway between the two ion cyclotron frequencies, namely,

$$\frac{4\,v}{\ell\,(\omega_{c1}-\omega_{c2})} < 1 \,. \qquad (11)$$

It should be noted that this analysis is restricted to single particle motion in an electrostatic field, and that no account has been made of collective effects. However, to obtain an estimate of the influence of transit-time effects in the LMP experiment, we consider eq. (11) with $\ell = \lambda_\parallel/4$ and $v = (2T_i/m_i)^{1/2}$. We then obtain, for an adiabatic response, the requirement

$$\frac{\lambda}{16}\,(\omega_{c1}-\omega_{c2})\left(\frac{m_i}{2\,T_i}\right)^{1/2} > 1 \,.$$

Substituting the appropriate values yields

$$\frac{\lambda}{16}\left(\omega_{c1}-\omega_{c2}\right)\left(\frac{m_i}{2T_i}\right)^{1/2} = 4\times 10^{3} > 1 .$$

We may therefore expect that for the experiment to be conducted on the LMP device, the ions respond adiabatically to the applied wave field, and transit-time effects are negligible.

E) Finite size of plasma

For the fluid description of the ponderomotive effect to be valid, we clearly require that the diameter of the plasma column must be much greater than the Larmor radius of the ions. Assuming no increase in the perpendicular temperature, we have

$$\rho_{ci} = \frac{1}{\omega_{ci}}\left(\frac{T_{\perp i}}{m_i}\right)^{1/2} = 6\cdot 8\times 10^{-2}\ \text{cm}$$

which is much less than the plasma radius, a = 2.5 cm. In fact, even in the presence of a substantial increase in perpendicular ion velocity, the condition $\rho_{ci} \ll a$ is not violated.

F) Finite lifetime of particles

The fluid description of the plasma assumes an equilibrium which is static. However, in an experimental device, the equilibrium is dynamic; ions and electrons are continually being created (by the source mechanism, e.g. cathode) and lost (by e.g. re-combination, boundary losses). For the plasma of the LMP device, being strongly magnetized and of low density, the major loss mechanism arises from the streaming of particles out the ends of the device. The transit time of particles across the length of the device defines a pseudo-collision frequency

$$\nu_{loss} = \frac{1}{\tau_{transit}} = \frac{V_{th}}{L} .$$

Substituting the appropriate values for the LMP device yields for the ions

$$\nu_{loss} \simeq 0.2 \text{ kHz}$$

Since this is much less than the ion-neutral collision frequency (~ 5 kHz), end-loss effects should not play a dominant role in determining the modified density distributions.

G) Stochasticity

It is well known that the orbits in phase space due to a ponderomotive potential can be destroyed by intrinsic stochasticity[36] which results in heating[37]. A condition for the onset of stochasticity can be obtained by using Chirikov's criterion of overlapping orbits[38].

In the field of an electromagnetic wave propagating parallel to the magnetic field, the ions may perform closed orbits[39]. The velocity at the separatrix is given by

$$v_{separatrix} = \frac{\omega - \omega_{ci}}{k_{\parallel}} ,$$

while the width of the orbits increases with the amplitude of the field. In the field of a standing wave, overlapping of orbits and intrinsic stochasticity can therefore occur[40]

- at a given field amplitude, if $(\omega-\omega_{ci})$ is small
- at a given value of $(\omega-\omega_{ci})$ if the wave amplitude is sufficiently large.

Figure 5 shows the ion trajectory in the field of a standing ion cyclotron wave in an infinite plasma. For $(\omega-\omega_{ci}) = 0.05\ \omega_{ci}$, and a wave amplitude of 1000 Vm^{-1}, the orbits of low energy ions are just

the familiar closed orbits. Keeping the frequency fixed, but increasing the field amplitude destroys these orbits (see Fig. 5b, for E_o = 3000 Vm^{-1}) and the ion motion become stochastic. A similar effect is obtained when (ω - ω_{ci}) is decreased to 0.02 ω_{ci} even for E_o = 1000 Vm^{-1} (see Fig. 5c, d).

The field amplitude at which intrinsic stochasticity may occur for our experimental condition ($\omega-\omega_{ci}$ = 0.05 ω_{ci}) exceeds the designed field by roughly an order of magnitude. Consequently, unless the field is drastically increased or the frequency is moved closer to ω_{ci}, the presence of intrinsic stochasticity should not be significant.

3. DIAGNOSTICS

A set of standard diagnostics will be installed on the LMP device:

i) Microwave interferometer (X and Ka bands)
   - to measure the electron density averaged across the plasma diameter.

ii) Langmuir probes
   - to obtain the radial profile of the density. Since the plasma is strongly magnetized, a reliable value of the magnitude of the density cannot be obtained from Langmuir probe measurements.

iii) Mass spectrometer
   - to measure the global ratio of ion concentration in a multi-ion species plasma.

iv) Passive spectroscopy
   - measurement of the Doppler broadening of ion lines yields the ion temperature.

v) Ion-acoustic wave
   - measurement of the propagation speed and damping yields values of the ion and electron temperature.

vi) Resonance cone

- the radiation of several types of plasma waves from a point source defines a resonance cone. Measurement of cone angles and fine structure can yield values for the electron density[41,42] and electron[41] and ion[43] temperatures.

vii) Magnetic probes

- small magnetic coils will be used to obtain spatial and temporal measurements of the magnetic fields associated with the ion cyclotron wave. In addition, a single turn coil placed around the plasma and under each Stix coil module (see fig. 4b) will measure the axial oscillating magnetic flux.

Associated with the proposed experimental investigation of the ponderomotive force in the LMP device, as discussed in section 2, are two complementary phenomena that may be observed:

- the modification of the isotopic concentration in a two-ion species plasma due to the sensitivity of the ponderomotive potential on the ion mass. This leads, in a steady state experiment, to a non-uniform static spatial distribution of the ratio of isotopic concentration.

- the non-linear plasma-wave interaction results in higher order components of the wave frequency spectrum. In particular, a second-order, double-frequency component of the wavefields should be produced. A theoretical study of the spatial behaviour of this component is presently being undertaken.

The second-order magnetic field associated with the large amplitude ion cyclotron wave should be readily detectable using magnetic probes, with phase-locked and frequency-selective signal processing. Regarding the measurement of the modification of the isotopic concentration, one notices that, as was remarked in section 2.2:

- the electron density (i.e. the total ion density) is not significantly modified by the ponderomotive force.

- the density of each isotope is strongly dependent on the spatial variation of the ponderomotive potential.

These two considerations necessitate a diagnostic which has a good spatial resolution and which is sensitive to ion mass. A cold probe, such as the one used in Reference 44, is not practical due to the low liquefaction point of neon ($T_{liquefaction} < 27\,^{\circ}K$) and low degree of ionization of the plasma. The use of a high permeability extraction tube inserted in the plasma, followed by the appropriate ion optics and a mass-sensitive detection system, greatly perturbs the static magnetic field and the ion cyclotron wavefield.

Laser-induced resonant fluorescence has been selected since it is a non-perturbing method with high spatial resolution[45,46]. The separation of the transition wave numbers for the two isotopes of neon is given approximately by

$$\Delta k \simeq k \left(\frac{1}{M_{20}} - \frac{1}{M_{22}} \right) \frac{1}{1836} ,$$

where $k = 1/\lambda$. For a transition wavelength around 370 nm, Δk is of the order of 0.065 cm^{-1}, corresponding to a separation in frequency of 2 GHz, and

$$\left.\frac{\Delta k}{k}\right|_{isotopic} = \left.\frac{\Delta \omega}{\omega}\right|_{isotopic} \simeq 2.4 \times 10^{-6} .$$

The Doppler width corresponding to an ion temperature of $2000\,^{\circ}K$ is

$$\left.\frac{\Delta k}{k}\right|_{Doppler} = \left.\frac{\Delta \omega}{\omega}\right|_{Doppler} = 7.2 \times 10^{-7} \left(\frac{T_i\,(^{\circ}K)}{A} \right)^{1/2}$$

$$= 7.2 \times 10^{-6} .$$

Since $\Delta\omega/\omega_{Doppler} > \Delta\omega/\omega_{isotopic}$, it is necessary to use a Doppler-free technique to obtain accurate measurements of the isotope concentration.

Doppler-free techniques can be classified into two main groups: one photon and many-photon spectroscopy[47]. All techniques require a laser beam with a frequency bandwidth that is much less than the Doppler width. One photon spectroscopy only involves that fraction of the ion population with velocity between $-\delta\omega/k$ and $+\delta\omega/k$, where $\delta\omega$ is the natural width of the transmission, which is usually much smaller than the Doppler width. However, for two-photon spectroscopy using two counter-propagating laser beams, all particles in the selected quantum state, regardless of their velocity, are able to absorb the energy of the two photons. Thus two-photon spectroscopy, having the advantage of a much stronger fluorescence signal, has been chosen for the measurement of isotopic concentration.

For singly-ionized neon, we have identified a few favourable transitions which can be excited by the absorption of two photons:

Initial state	Final state	Vacuum wavelength	
$(^3P)\ 3p\ ^2P_{3/2}$	$(^3P)\ 5p\ ^4D_{3/2}$	373.0668 nm	
$(^3P)\ 3p\ ^2P_{3/2}$	$(^3P)\ 5p\ ^4S_{3/2}$	370.5633 nm	(preferred transition)
$(^3P)\ 3p\ ^2P_{3/2}$	$(^3P)\ 5p\ ^2D_{5/2}$	372.2327 nm	

The most favourable decay lines are at 363.4 nm, 317.8 nm and 367.6 nm, respectively. To perform the measurement, a Lambda Physik Pulsed Dye Laser was selected. In the vicinity of 370 nm, its characteristics are: Pulse length ≈ 10 ns, Energy = 8 mJ, Line width ≈ 200 MHz.

By spatially scanning the laser beam, the profile of the density of each isotope may be obtained in the presence and in the absence of the ponderomotive force. According to the theoretical calculations[29], the concentration of the minority species may be enhanced by as much as a factor three from the unperturbed value: such a change should be detectable.

Laser fluorescence may also be used to monitor, by an optical tagging technique,[48] the diffusion of ions in the plasma. This technique uses the observation of the fluorescence from a metastable state in ions that have been excited at a different spatial location. Sodium ions $(Na^{23})^+$, having easily pumped, long lived metastable states, appear to be a suitable choice to closely model the behaviour of the minority $(Ne^{22})^+$ ions. The relative importance of radial and axial diffusion due to the ponderomotive force could therefore be examined.

Acknowledgements

The authors gratefully acknowledge the contributions of the drafting office, in particular the efforts of P. Gorgerat, and the vacuum, mechanical, electrical and electronics workshops in the design and construction of the LMP device. They are also grateful to M.C. Festeau-Barrioz for providing the numerical calculations shown in Fig. 5.

This work has been supported by the Ecole Polytechnique Fédérale de Lausanne, the Swiss National Science Foundation and by Euratom.

References

1. Motley, R.W., Q Machines, Academic Press (1975).

2. Lisitano, G., Fontanesi, M. and Sindoni, E., Appl. Phys. Lett., 16, 122 (1970).

3. Bitter, M., Hollenstein, Ch. and Paris, P.J., Rev. Sci. Instrum., 47, 1209 (1976).

4. Janzen, G. and Räuchle, E., Phys. Lett., 83A, 15 (1981).

5. Hirshfield, J.L., Jacob, J.H. and Baldwin, D.E., Phys. Fluids, 14, 615 (1971).

6. Gekelman, W. and Stenzel, R.L., Rev. Sci. Instrum., 46, 1386 (1975).

7. Ono, M., Porkolab, M. and Chang, R.P.H., Phys. Fluids, 23, 1656 (1980).

8. Statham, G. and ter Haar, D., University of Oxford Report 17/82 (1982).

9. Pitaevskii, L.P., Sov. Phys. JETP, 12, 1008 (1961).

10. Washimi, H. and Karpman, V.I., Sov. Phys. JETP, 44, 528 (1976).

11. Kono, M., Skoric, M.M. and ter Haar, D., J. Plasma Phys., 26, 123 (1981).

12. Kaufmann, A.N. and Stenflo, L., Phys. Scripta, 11, 269 (1975).

13. Porkolab, M. and Goldman, M.V., Phys. Fluids, 19, 872 (1976).

14. Cary, J.R. and Kaufmann, A.N., Phys. Rev. Lett., 39, 402 (1977).

15. Cary. J.R. and Kaufmann, A.N., Phys. Fluids, 24, 1238 (1981).

16. Motz, H. and Watson, C.J.H., Adv. Electronics Electron Phys., 23, 153 (1967).

17. Cary, J.R. and Hammer, J.H., Comments Plasma Phys. Cont. Fusion, 5, 159 (1979).

18. Akiyama, H. Matsumoto, O. and Takeda, S., Proc. 9th Europ. Conf. on Contr. Fusion and Plasma Phys., Oxford, AP31, 38 (1979).

19. Sanuki, H., Nagoya Uni. Report, IPPJ-558 (1982).

20. Watari. T., Hiroe, S., Sato, T. and Ichimaru, S., Phys. Fluids, 17, 2107 (1974).

21. Hiroe, S. et al. Phys. Fluids, 21, 676 (1978).

22. Watari, T. et al., Phys. Fluids, 21, 2076 (1978).

23. Fader, W.J., Jong, R.A., Stufflebeam, J.H. and Sziklas, E.A., Phys. Rev. Lett., 46, 999 (1981).

24. Sato, T. et al., Comments Plasma Phys. Cont. Fusion, 7, 131 (1982).

25. Hidekuma, S. et al., Phys. Rev. Lett., 33, 1537 (1974).

26. Hiroe, S. et al., Nucl. Fusion, 15, 769 (1975).

27. Weibel, E.S., Phys. Rev. Lett., 44, 377 (1980).

28. Festeau-Barrioz, M.C. and Weibel, E.S., Phys. Fluids, 23, 2045 (1980).

29. Weibel, E.S. and Festeau-Barrioz, M.C., Plasma Phys., 24, 243 (1982).
Festeau-Barrioz, M.C. and Weibel, E.S., Comput. Phys. Commun., 27, 11 (1982).

30. Sawley, M.L. and Tran, M.Q., Lausanne Report, LRP 206/82 (1982).

31. Dodge, N.B., Kristiansen, M. and Dougal, A.A., Rev. Sci. Instrum., 37, 1455 (1966).

32. Stix, T.H., Nucl. Fusion, 15, 737 (1975).

33. Spitzer, L., Physics of Fully Ionized Gases, Interscience (1962).

34. Dimonte, G., Lamb, B.M. and Morales, G.J., Phys. Rev. Lett. 48, 1352 (1982).

35. Dimonte, G., Lamb, B.M. and Morales, G.J., U.C.L.A. Report, PPG- (1982).

36. Schmidt, G., Comments Plasma Phys. Cont. Fusion, 7, 87 (1982).

37. Doveil, F., Phys. Rev. Lett., 46, 532 (1981).

38. Zaslavskii, G.M. and Chirikov, B.V., Sov. Phys. Uspekii, 14, 549 (1972).

39. Laird, M.J. and Knox, F.B., Phys. Fluids, 8, 755 (1965).

40. Tran, M.Q., IEEE Trans. Plasma Sci. PS10, 16 (1982).

41. Fisher, R.K. and Gould, R.W., Phys. Fluids, 14, 857 (1971).

42. Ichovic, J., Stenzel, R.L. and Gekelman, W., Rev. Sci. Instrum., 48, 485 (1977).

43. Ohnuma, T. Kuwabara, T., Shibata, K. and Adachi, S., Phys. Rev. Lett., 37, 206 (1976).

44. Dawson, J.M. et al., Phys. Rev. Lett., 37, 1547 (1976).

45. Stern, R.A. and Johnson, J.A., Phys. Rev. Lett., 34, 1548 (1975).

46. Muller, C.M. and Burrel, K.H., Phys. Rev. Lett., 47, 330 (1981).

47. Letokhov, V.S. and Chebotayev, V.P., Nonlinear Laser Spectroscopy, Springer-Verlag (1977).

48. Stern, R.A., Hill, D.N. and Rynn, N., Phys. Rev. Lett. 47, 792 (1981).

Figure Captions

Fig. 1 : General view of the LMP device.

Fig. 2 : Magnetic field coil design.

Fig. 3 : Cathode design.

Fig. 4 : a) Schematic diagram of the wave antenna circuit.

b) Sketch of the prototype of an antenna module.

Fig. 5 : Phase-space trajectories of an ion in the field of a standing ion cyclotron wave

a) $(\omega-\omega_{ci}) = 0.05\ \omega_{ci}$; $E_o = 1000\ V\ m^{-1}$
b) $(\omega-\omega_{ci}) = 0.05\ \omega_{ci}$; $E_o = 3000\ V\ m^{-1}$
c) $(\omega-\omega_{ci}) = 0.02\ \omega_{ci}$; $E_o = 1000\ V\ m^{-1}$
d) $(\omega-\omega_{ci}) = 0.02\ \omega_{ci}$; $E_o = 3000\ V\ m^{-1}$

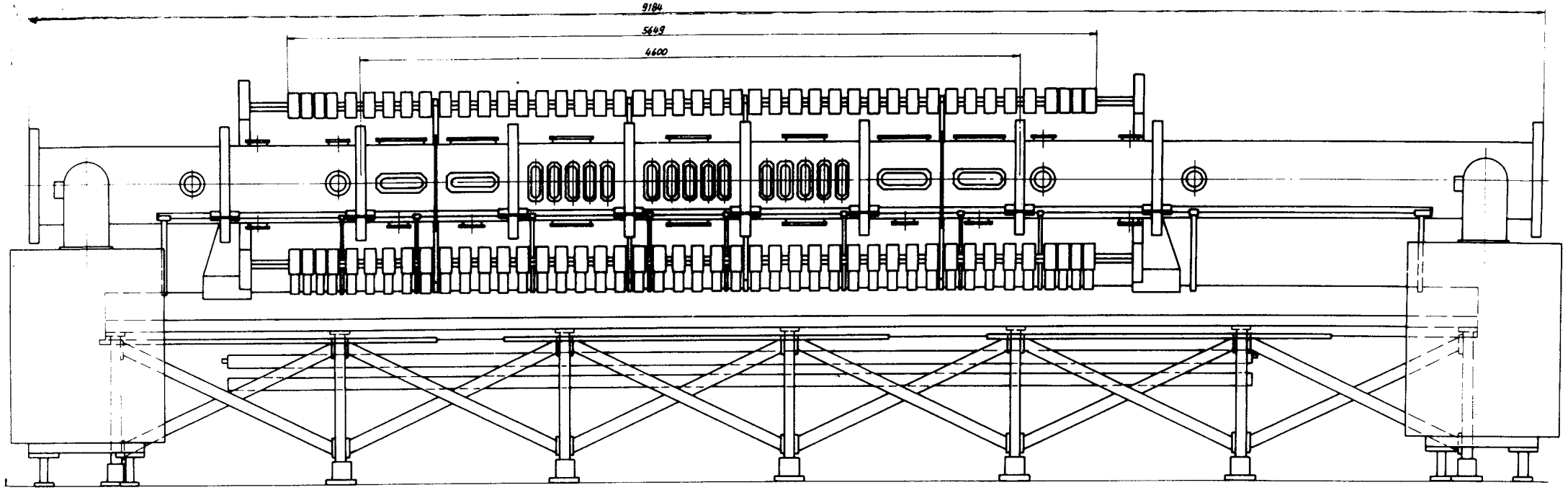

FIG. 1

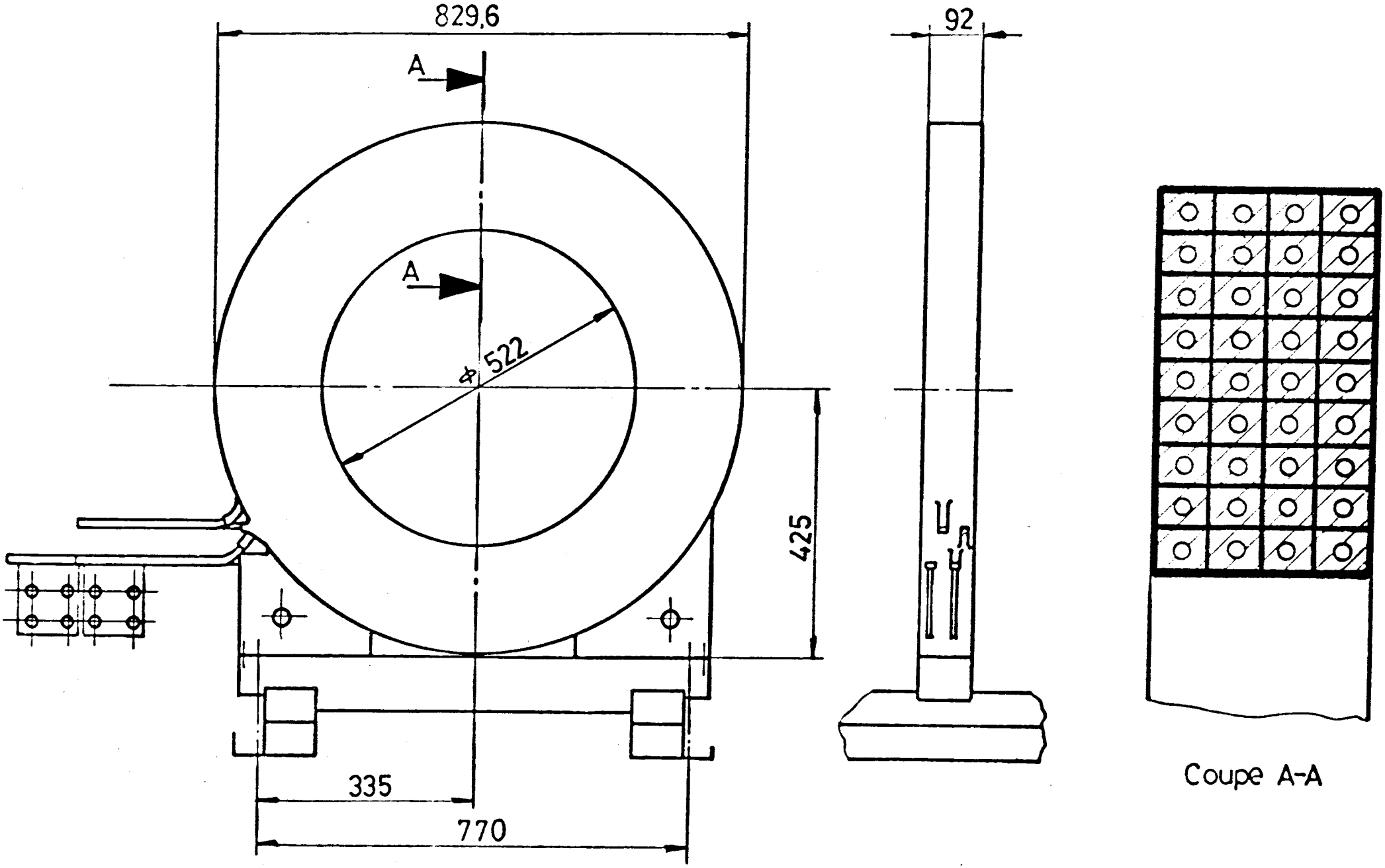

FIG. 2

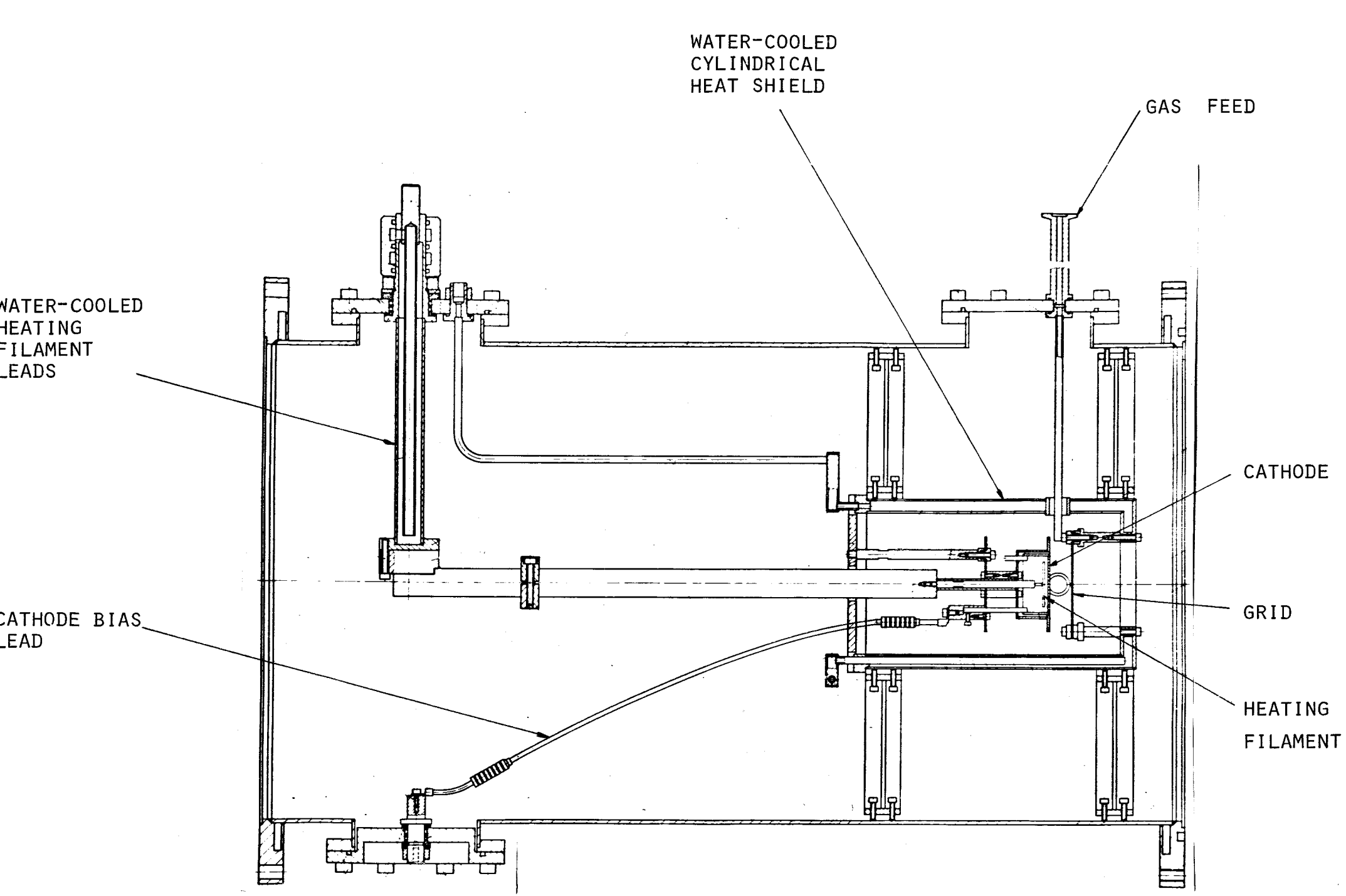
WATER-COOLED
CYLINDRICAL
HEAT SHIELD
GAS FEED
WATER-COOLED
HEATING
FILAMENT
LEADS
CATHODE
GRID
CATHODE BIAS
LEAD
HEATING
FILAMENT

FIG. 3

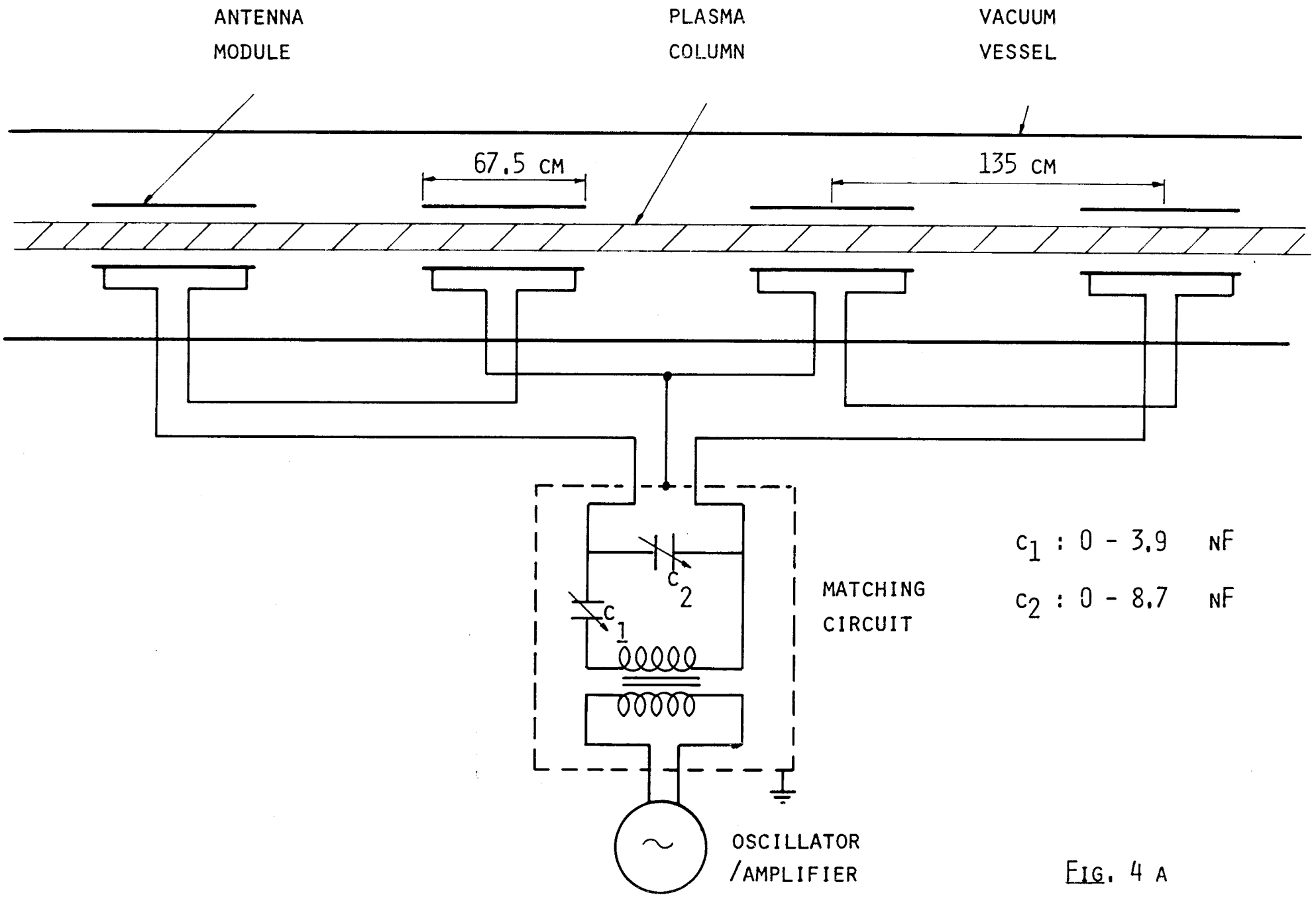

C_1 : 0 - 3,9 NF

C_2 : 0 - 8,7 NF

FIG. 4 A

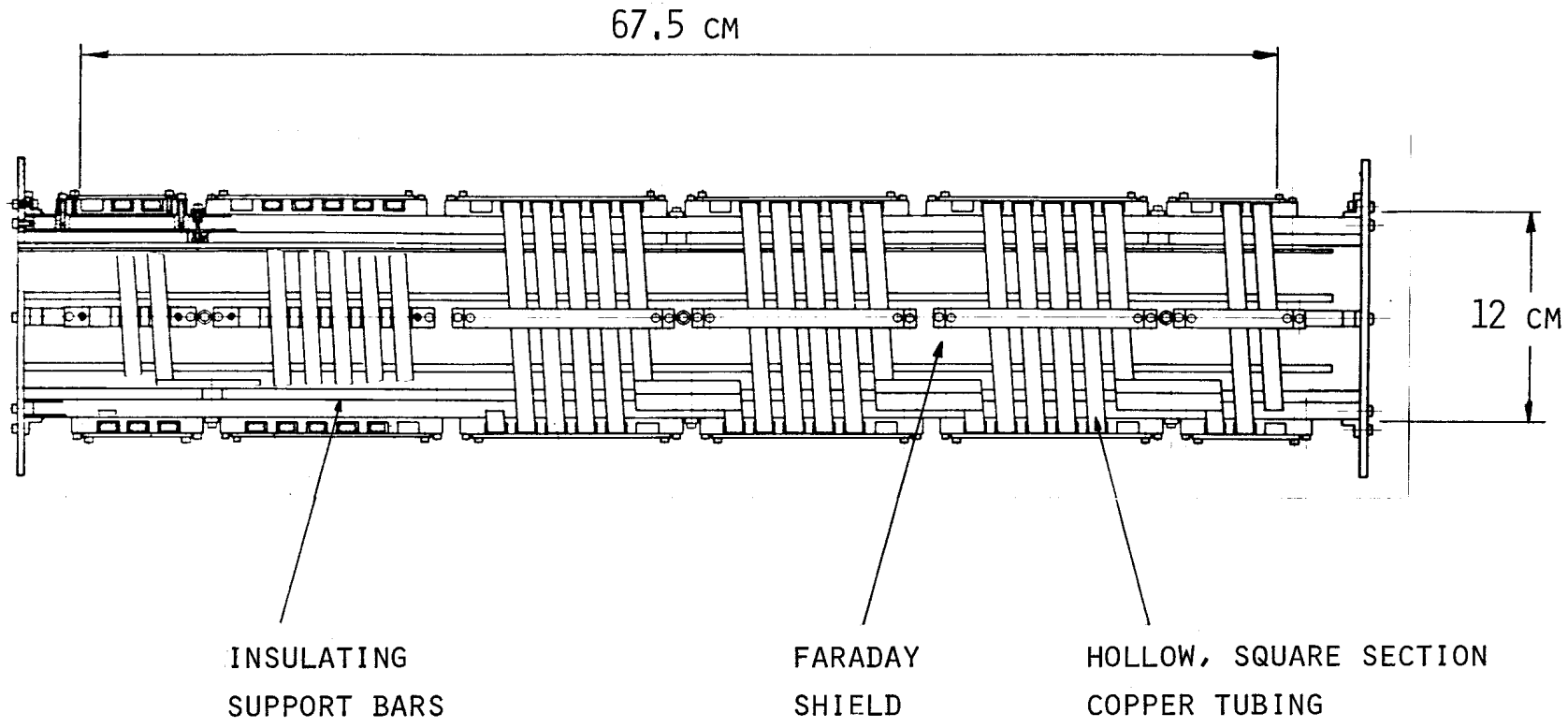
67.5 CM
12 CM
INSULATING
SUPPORT BARS
FARADAY
SHIELD
HOLLOW, SQUARE SECTION
COPPER TUBING

FIG. 4 B

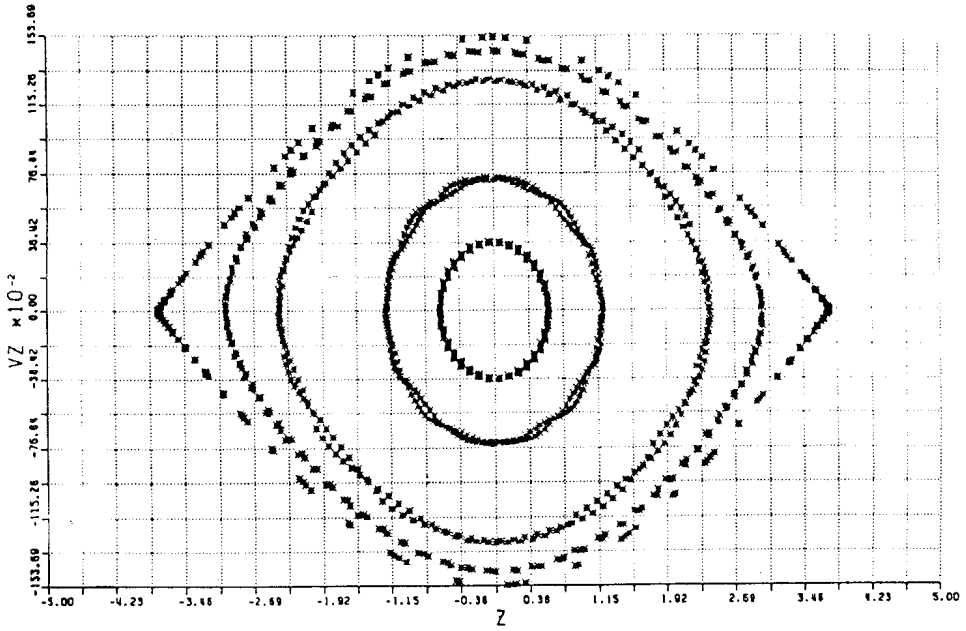

A)

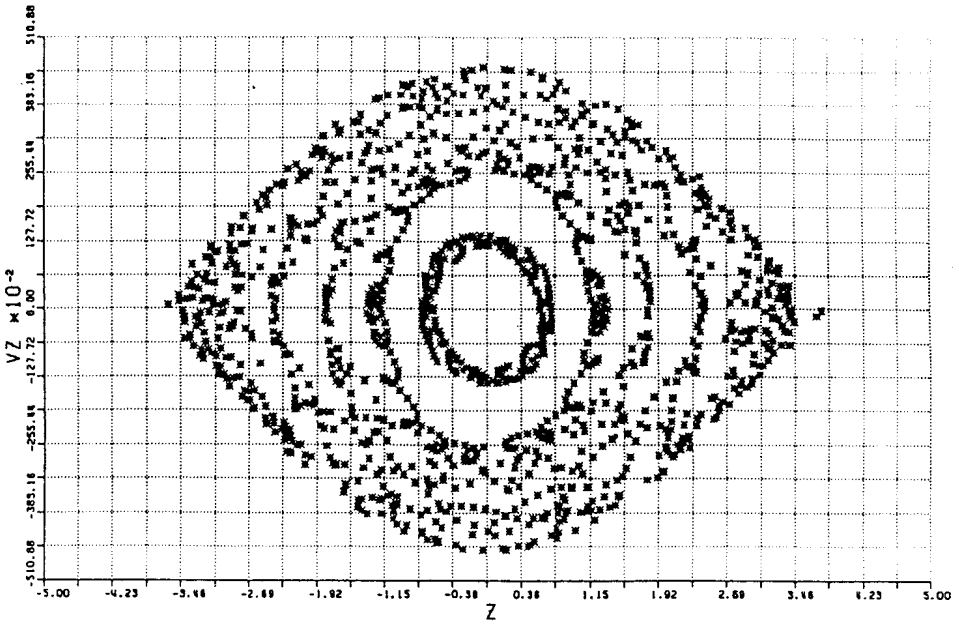

B)

C)

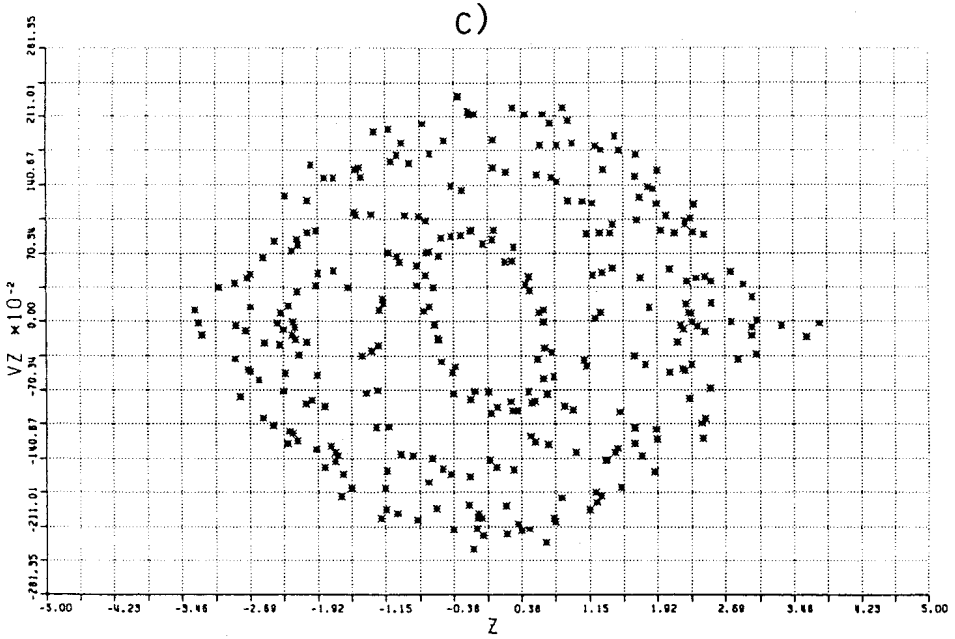

D)

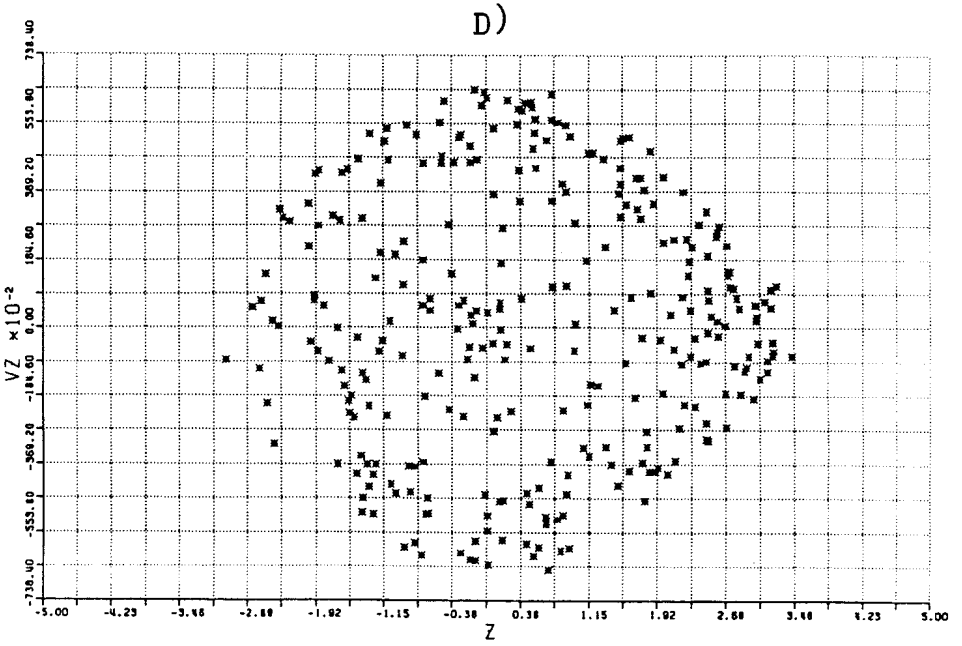

FIG. 5